Silicon (2024) 16:4635–4645
https://doi.org/10.1007/s12633-024-03035-3

RESEARCH

Structural and Optical Properties of $Bi_4Si_{x/2}Ge_{x/2}V_{2-x}O_{11-x/2}$ Compounds: Effect of Double Substitution and Phase Transitions

A. Agnaou[1] · W. Mhaira[1] · R. Essalim[1] · M. Zaghrioui[2] · T. Chartier[2] · C. Autret[2] · A. Ammar[1]

Received: 30 March 2024 / Accepted: 23 May 2024 / Published online: 28 May 2024

Abstract

The solid-state reaction method was employed to successfully synthesize a range of compounds, $Bi_4Si_{x/2}Ge_{x/2}V_{2-x}O_{11-x/2}$, where $0.1 \leq x \leq 0.6$. The main aim of this investigation is to examine how the structural and optical properties are influenced by the double substitution on vanadium site. The analyses using room temperature X-ray diffraction (XRD) revealed existence of α-monoclinic and β-orthorhombic phases in the composition range of $0.1 \leq x \leq 0.3$ and $0.4 \leq x \leq 0.5$, respectively. The α to β structural transition, as a function of the substitution rate, was further confirmed through Raman and infrared spectroscopies at room temperature, which both verified the presence of these two distinct phases depending on the composition. The X-ray diffraction (XRD) analysis, versus temperature, highlighted the $\alpha \rightarrow \beta$ and $\beta \rightarrow \gamma$ phase transitions with increasing the temperature. These phase transitions were confirmed by DTA and Raman investigations as a function of temperature. Diffuse reflectance spectroscopy showed that the band gap varies around 2.1eV and that the compound with $x = 0.1$ has the lowest value of 2.08 eV.

Keywords BiSiGeVOx · XRD as a function of temperature · DTA · Raman spectroscopy · Optical properties

1 Introduction

A fascinating class of layered perovskite known as Aurivillius phases [1] has garnered considerable attention due to their diverse chemical properties [2, 3]. These compounds feature a unique structure composed of alternating fluorite-like $[Bi_2O_2]^{2+}$ layers and perovskite-like $[A_{n-1}B_nO_{3n+1}]^{2-}$ layers, forming a regular intergrowth. In our pursuit of novel and highly active catalytic systems, we have turned our focus to the bismuth and vanadium-based mixed oxides known primarily for their exceptional anionic conductivity via oxide ions. Among these, $Bi_4V_2O_{11}$ stands out as a compound with a significant number of oxygen vacancies, which contributes to its excellent conductivity.

Depending on the temperature, $Bi_4V_2O_{11}$ exhibits three distinct crystalline phases: the α-monoclinic phase (below 450 °C), the β-orthorhombic phase (between 450 and 570 °C), and the γ-tetragonal phase (above 570 °C) [4, 5]. Notably, the γ-phase, achieved at high temperatures, displays the highest conductivity surpassing 10^{-1} S.cm^{-1} [6–8]. These various polymorphs can be explained by referencing the orthorhombic cell, which possesses average dimensions of $a_m \approx 5.53$ Å, $b_m \approx 5.61$ Å, and $c_m \approx 15.28$ Å [9, 10].

By introducing cations through single or double partial substitution of vanadium, researchers have successfully achieved the stabilization of the high-temperature γ phase at room temperature, leading to the development of highly conductive electrolytes. This exciting advancement has given rise to a novel class of materials known as BiMeVOx, derived from the formulation $Bi_4Me_xV_{2-x}O_{11-\delta}$ (Bismuth Metal Vanadium Oxide). The BiMeVOx compounds have garnered significant attention due to their exceptional polar properties, applications in oxygen-separation membranes, and impressive ionic conductivity [11–15].

In a previous study [16], we demonstrated that the substitution of vanadium (V^{V}) with silicon (Si^{IV}) in the solid solution $Bi_4Si_xV_{2-x}O_{11-x/2}$ ($0.0 \leq x \leq 0.4$) resulted in the stabilization of the γ-tetragonal phase of $Bi_4V_2O_{11}$. This substitution led to notable conductivity values, reaching approximately 10^{-5} S.cm^{-1} at 300 °C and 10^{-2} S.cm^{-1} at

---

✉ A. Agnaou
a.agnaou.ced@uca.ac.ma

[1] Laboratory of Materials Science and Process Optimization, Faculty of Science-Semlalia, Cadi Ayyad University, Av. My Abdellah, B.P. 2390, Marrakech, Morocco

[2] Laboratoire GREMAN UMR 7347, Université de Tours, 15 rue de la Chocolaterie, 41 000 Blois, France

600 °C for the composition with x = 0.1. Conversely, in the case of the solid solution BiSiPVOx ($0.0 \leq x \leq 0.5$) that we synthesized in a previous work [17], the double substitution of vanadium (V^V) with silicon (Si^{IV}) and phosphorus (P^V) failed to stabilize the γ-tetragonal phase of $Bi_4V_2O_{11}$. Despite this, the composition with x = 0.1 displayed a higher conductivity of approximately 2.6×10^{-3} $S.cm^{-1}$ at 600 °C [17]. Additionally, Yue et al. [18] synthesized the solid solution $Bi_2Ge_xV_{1-x}O_{5.5-\delta}$ ($0.0 \leq x \leq 0.5$), where the γ-tetragonal phase of $Bi_4V_2O_{11}$ was successfully stabilized at low temperatures. For this particular composition, x = 0.35, the conductivity was around 10^{-2} $S.cm^{-1}$ at 600 °C.

In addition to their exceptional conduction properties, this group of compounds has begun in recent years to occupy a predominant place among the low gap energy photo-catalysts which are of great interest to many researchers. The compound $Bi_4V_2O_{11}$ is a semiconductor that can absorb the sunlight due to its band gap higher than 2 eV. The band gap energy of $Bi_4V_2O_{11}$ reported by Anwar et al. is of 2.86 eV [19]. Moreover, we have shown, in recent studies [20–22], that the double substitution of vanadium in $Bi_4V_2O_{11}$ leads to a narrower band gap for all of the studied phases Bi(Si,Co)VOx, Bi(Si,Cu)VOx, Bi(Cu,Sb)VOx and Bi(Si,P)VOx.

Our work is part of an approach aimed at studying BiMeVOx obtained by double substitution with elements from block p of the periodic table. The main objective of this study is to improve the optical performance of the $Bi_4V_2O_{11}$ phase by creating defects likely to reduce the gap energy of this material and also to highlight the effect of the nature of the doping elements chosen on structural properties in relation to the strength and nature of the bonds within the material.

In this current investigation, the simultaneous substitution of vanadium in the mother phase $Bi_4V_2O_{11}$ was carried out using silicon (Si^{4+}) and germanium (Ge^{4+}), resulting in the formation of the solid solution $Bi_4Si_{x/2}Ge_{x/2}V_{2-x}O_{11-x/2}$. Various analytical techniques, such as X-ray diffraction (XRD), FTIR, and Raman spectroscopy, were employed to comprehensively characterize the synthesized BiSiGeVOx sample. Additionally, analysis involving XRD and Raman at different temperatures, scanning electron microscopy (SEM), and diffuse reflectance spectroscopy (DRS) were conducted. These characterization methods were employed to gain insights into the structural properties, vibrational modes, surface morphology, and optical properties of the BiSiGeVOx solid solution.

2 Experimental

Polycrystalline samples of $Bi_4Si_{x/2}Ge_{x/2}V_{2-x}O_{11-x/2}$ (with $0.1 \leq x \leq 0.6$) were prepared using a conventional solid-state reaction method. High-purity Bi_2O_3 (99.5%), V_2O_5 (99%), SiO_2 (99.9%), and GeO_2 (99.998%) were accurately weighed and ground for 20 min. The resulting mixture was then heated at 800 °C for 24 h under ambient air conditions to promote the formation of the desired compounds. Part of synthesized powder was used to prepare pellets. These were sintered at 840 °C for 5 h.

To characterize the powder samples, a Rigaku SmartLab SE powder diffractometer was utilized for X-ray diffraction (XRD) analysis. Kα radiation with a copper wavelength ($\lambda = 1.54056$ Å) was employed, and the 2θ range was scanned from 5° to 65° with a step size of 0.02°, and a scanning speed of 2°/min. Differential thermal analysis was performed on powdered samples in an air environment, from 20°C to 800°C at a heating rate of 10°C/min, utilizing a NETZSCH STA 2500 instrument. Raman scattering spectra were acquired using a Renishaw Invia Reflex spectrometer equipped with a He Laser (632.8 nm). The incident light was focused on sample using × 50 lens and the scattered light, collected in the backscattering configuration, was dispersed with a 1800 lines/mm grating before reaching the CCD camera. The Linkam THMS600 stage and its temperature controller were employed for temperature-dependent Raman spectra. At each temperature the spectrum was recorded 10 min after the target temperature is reached. The infrared study was conducted in transmission mode using a Fourier transform (FTIR) spectrometer of VERTEX 70 type. Measurements were carried out in the spectral range of 4000 to 400 cm^{-1} on homogeneous KBr pellets with a 2/100 ratio between sample and KBr. We subsequently examined them under the microscope using the “VEGA3” instrument, equipped with an advanced energy-dispersive X-ray spectroscopy (EDS) analyzer. After sintering the ceramics at a temperature of 840 °C for 5 h, we conducted a detailed examination to assess the surface characteristics and identify the elemental composition present in the samples. We used diffuse reflectance spectroscopy (DRS) to investigate the optical properties of the powdered samples at room temperature, in the UV–Visible spectral range (200 to 800 nm) using a Shimadzu spectrophotometer (UV-3101).

3 Results and Discussion

3.1 X-ray Diffraction and Differential Thermal Analysis

Figure 1 illustrates the diffractograms obtained for the $Bi_4Si_{x/2}Ge_{x/2}V_{2-x}O_{11-x/2}$ ($0.1 \leq x \leq 0.6$) powders at room temperature. These diagrams show the formation of the BiSiGeVOx solid solution for $x \leq 0$. For the $Bi_4Si_{x/2}Ge_{x/2}V_{2-x}O_{11-x/2}$ solid solution with a substitution rate $x \leq 0.3$ (i.e., substitution rate ≤ 15%), the diffractograms exhibit distinctive features. Indeed, the diagrams

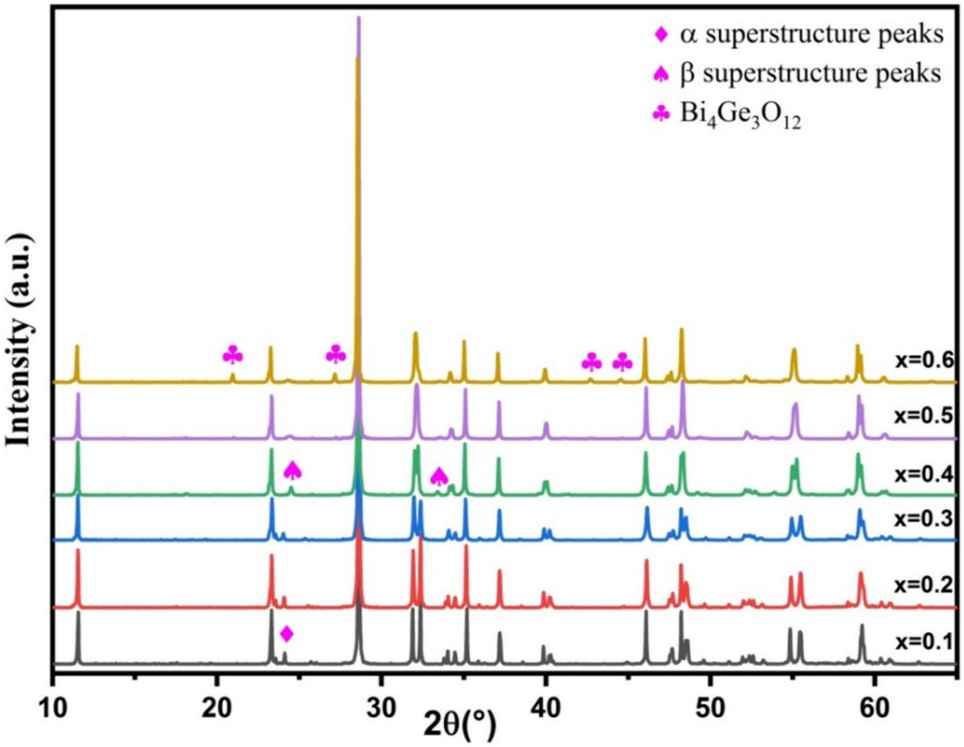

Fig. 1 X-ray diffractogram of $Bi_4Si_{x/2}Ge_{x/2}V_{2-x}O_{11-x/2}$

display a superstructure peak (indicated by ♦) at 2θ = 24.2° and doublets at 2θ = 32, 34, 40, 48, and 55°, signature of the α-monoclinic phase of BiMeVOx with *C2/m* space group. In the case of the $Bi_4Si_{x/2}Ge_{x/2}V_{2-x}O_{11-x/2}$ solid solution with a substitution ratio x = 0.4 and 0.5, the XRD diffractograms reveal the existence of superstructure peaks (indicated by ♠) at 2θ = 24.6° and 2θ = 33.3°, indicating the formation of the orthorhombic β-type BiMeVOx phase with *Amam* space group. However, when the substitution ratio exceeds this range, as seen in the XRD diffractogram for x = 0.6, additional peaks (indicated by ♣) appear at 2θ = 20.99° and 27.24°, corresponding to the secondary phase $Bi_4Ge_3O_{12}$ [18, 23]. Hence, the solid solution limit for $Bi_4Si_{x/2}Ge_{x/2}V_{2-x}O_{11-x/2}$ is observed at x≈0.6. Note that the tetragonal γ-phase of $Bi_4V_2O_{11}$ was not stabilized throughout the BiSiGeVOx solid solution domain. The same result was obtained in our previous works on the BiSiPVOx [17] and BiPVOx [24] solid solutions and in the BiGeVOx solid solution synthesized by Yue et al. [18]. However, we obtained a γ-tetragonal phase in the case of the mono-substituted silicon solid solution BiSiVOx only for x = 0.35 [16]. The strong covalent character of the P-O bond, which is not compatible with the disordered structure of the γ- form, can explain this behavior in BiSiPVOx and BiPVOx solid solutions. However, in the case of BiGeVOx and BiSiGeVOx solid solutions, the non-stabilization of the γ-form is probably due to the preferential tendency of germanium to adopt a tetrahedral environment in oxide systems.

The variations in lattice parameters and crystallite size with respect to the composition are summarized in Table 1. To facilitate comparison and enhance clarity, all lattice parameters have been converted to the orthorhombic mean cell using the relationship a ≈ 3 a_m, b ≈ b_m, and c ≈ c_m for the α-monoclinic phase. As the value of x increases, the *c*-axis parameter generally exhibits an upward trend, while *a* and *b* axes tend to approach each other, and the cell volume demonstrates fluctuations within the regions corresponding to the α and β phases. These variations cannot be explained by the differences in ionic radii between vanadium (0.54 Å) and silicon (0.26 Å in 4-coordination and 0.40 Å in 6-coordination), and germanium (0.39 Å in 4-coordination and 0.53 Å in 6-coordination) [25]. The expansion of the crystal lattice along the *c* direction indicates a decrease in the interaction between the vanadate and the bismuthate layers. Similar observations have been made in other compounds such as BiSiVOx [16], BiGeVOx [18, 23], and BiSiGaVOx [26]. The increase in the parameter *c* can also be explained by a

Table 1 Lattice parameters of the compounds $Bi_4Si_{x/2}Ge_{x/2}V_{2-x}O_{11-\delta}$

x	a(Å)	b(Å)	c(Å)	V(Å^3)	β(°)
0.1	5.5381	5.6090	15.2947	473.4993	94.708
0.2	5.5387	5.6011	15.2971	473.0968	94.499
0.3	5.5479	5.5908	15.3377	474.5457	94.048
0.4	5.5562	5.5869	15.3454	476.3509	90
0.5	5.5635	5.5789	15.3523	476.5079	90

stretching of the octahedral in the perovskite layers because of a ferroelectric displacement of the Si^{4+} ions.

Figures 2 and 3 show XRD plots as a function of temperature for the BiSiGeVOx solid solution with x = 0.1 and 0.4, respectively. For T ≤ 450 °C, the XRD diagram of the sample with x = 0.1 (Fig. 2) shows superstructure peaks at 2θ = 24.4 (indicated by ◆), which characterize the α-monoclinic phase (*C2/m* space group). At temperatures between 450 and 500 °C, the sample shows superstructure peaks at 2θ = 24.6 and 33.3° (indicated by ♠), which

Fig. 2 XRD patterns of $Bi_4Si_{0.05}Ge_{0.05}V_{1.90}O_{10.95}$ at different temperature

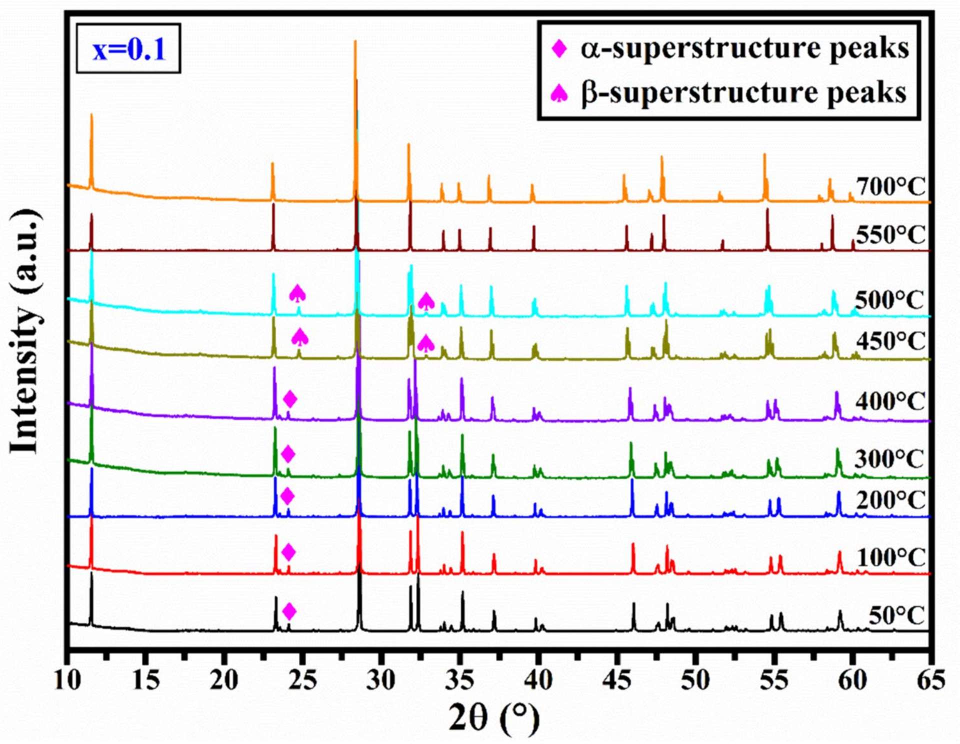

Fig. 3 XRD patterns of $Bi_4Si_{0.2}Ge_{0.2}V_{1.6}O_{10.8}$ at different temperature

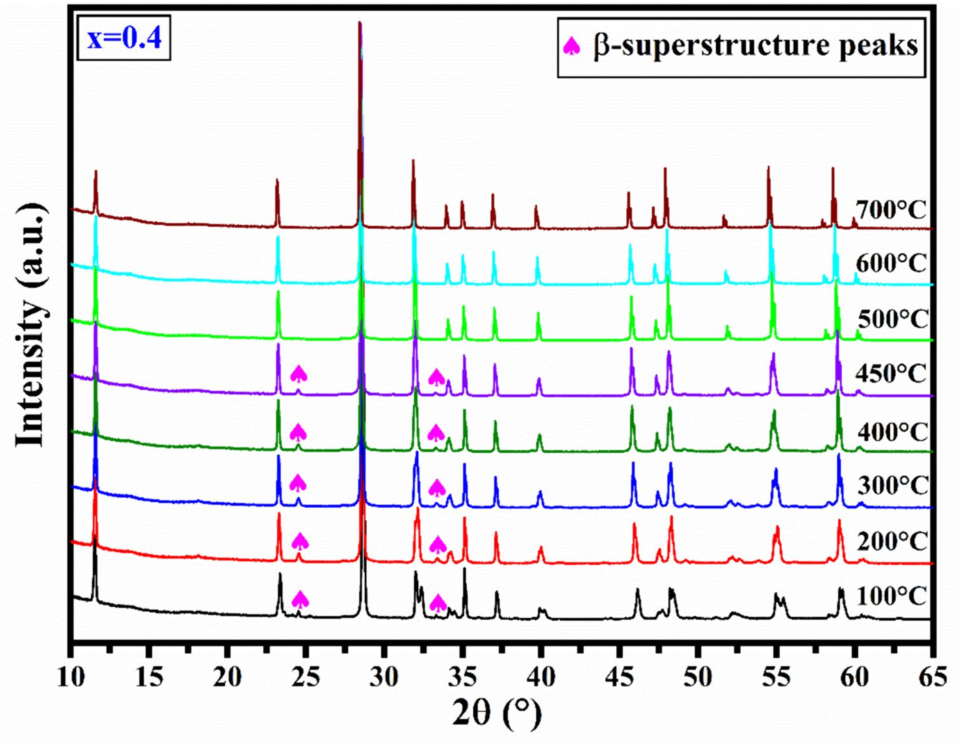

characterize the β-orthorhombic phase (*Amam* space group). Above 500 °C, the sample is completely transformed into the disordered γ-tetragonal phase (*I4/mmm* space group). For $x = 0.4$ (Fig. 3), the XRD diagram of the sample shows at $T \leq 450$ °C the presence of superstructure peaks at $2\theta = 24.6$ and 33.3° (indicated by ♠), which are characteristic of the β-orthorhombic phase (*Amam* space group). However, above 450 °C, the sample adopts the γ-tetragonal phase (*I4/mmm* space group).

The evolution of cell parameters and volume as a function of temperature for the BiSiGeVOx solid solution with $x = 0.1$ and 0.4 is illustrated in Figs. 4 and 5, respectively. For $x = 0.1$ and $x = 0.4$, *a* cell parameter increases, while *b* cell parameter decreases with increasing temperature up to $T = 500$ °C and 450 °C respectively. Above these temperatures, *a* and *b* parameters become equal signature of the γ-tetragonal phase. In addition, *c* parameter and cell volume increase progressively with temperature. It should be noted that *c* parameter undergoes a sudden increase at the β → γ phase transition, which can be explained by the movement of atoms in the crystal lattice linked to this structural transition [27].

Figure 6 shows the differential thermal analysis curve for BiSiGeVOx samples with $x = 0.1$ (α-phase) and $x = 0.4$ (β-phase). The DTA curve for $x = 0.1$ shows two endothermic peaks at 454 and 548 °C, representing α → β and β → γ phase transitions, respectively. For $x = 0.4$, the endothermic peak at 490 °C corresponds to the β → γ phase transition. These results are consistent with those obtained by XRD analyses.

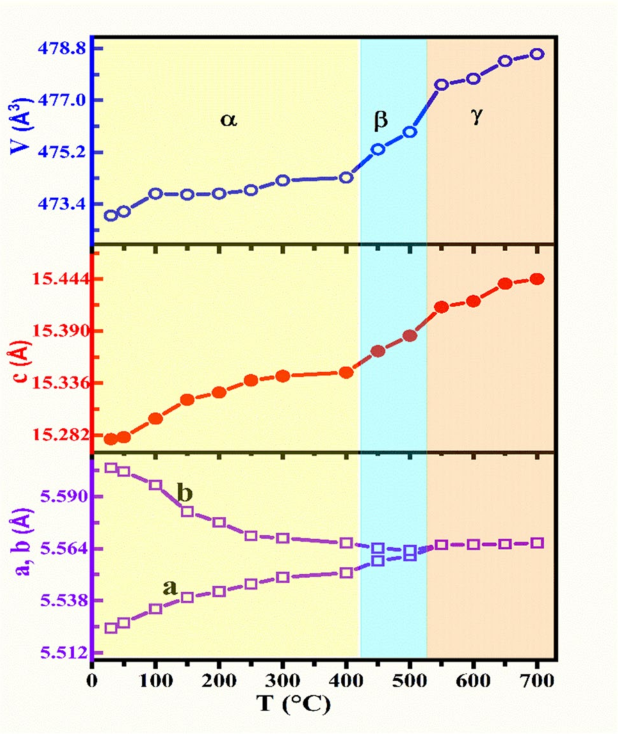

Fig. 4 Evolution of the lattice parameters and the cell volume as function of temperature for (**a**) $Bi_4Si_{0.05}Ge_{0.05}V_{1.90}O_{10.95}$ and (**b**) $Bi_4Si_{0.2}Ge_{0.2}V_{1.6}O_{10.8}$

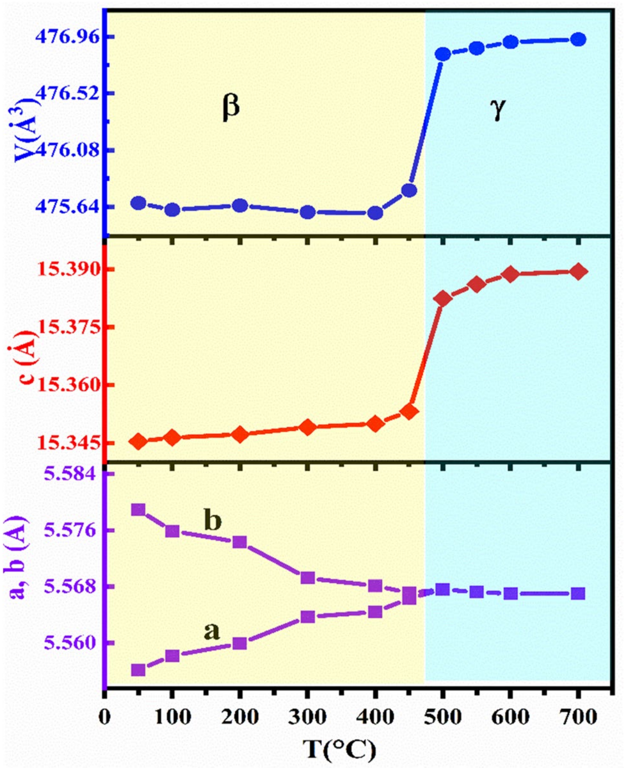

Fig. 5 Evolution of the lattice parameters and the cell volume of $Bi_4Si_{0.2}Ge_{0.2}V_{1.6}O_{10.8}$ as function of temperature

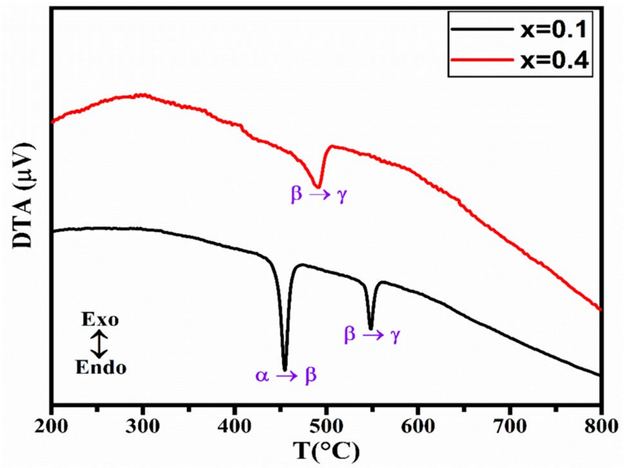

Fig. 6 DTA curves of $Bi_4Si_{x/2}Ge_{x/2}V_{2-x}O_{11-x/2}$

3.2 FTIR and Raman Spectroscopy

Figure 7 presents the transmission-mode FTIR spectra of the BiSiGeVOx system in the range of 4000–400 cm^{-1}. The bands located at 1636 cm^{-1} and 3430 cm^{-1} are assigned to the vibrational modes of the O–H bonds of water molecules hanging out on the samples. The bands around 613–617 cm^{-1} and 420 cm^{-1} are all attributed to the Bi-O bond stretching in the octahedral BiO_6 [28–30]. The band around 521–518 cm^{-1} is mainly associated with the stretching vibrations of the Bi-O bond in BiO_4 octahedral units [31], as well as the δ_{as} (O-V–O) deformation of vanadate ions [32]. The bands around 725–720 cm^{-1} and 829–812 cm^{-1} correspond to the symmetric and asymmetric stretching vibrations of V-O_A bonds (O_A: oxygen in apical position) [29, 32]. Moreover, when comparing the spectra of the samples crystallizing in the α-monoclinic phase ($x \leq 0.3$) with those adopting the β-orthorhombic structure ($x \geq 0.4$), it is evident to see that the bands at 768 cm^{-1}, 613–617 cm^{-1}, and 420 cm^{-1} completely disappear in the β-phase [17, 31, 33]. This disappearance can be attributed to the suppression of phonon modes resulting from a change in symmetry and then to a structural transition. The diminution of the mode number strongly suggests an increase of the symmetry, which is in agreement with α → β phase transition and the results obtained above (XRD and DTA).

Raman spectra of the solid solution $Bi_4Si_{x/2}Ge_{x/2}V_{2-x}O_{11-\delta}$ ($0.1 \leq x \leq 0.5$) at room temperature are presented in Fig. 8.

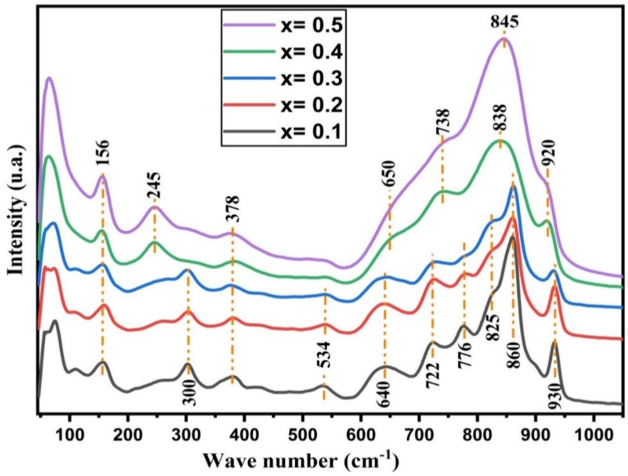

Fig. 8 Room temperature Raman spectra of $Bi_4Si_{x/2}Ge_{x/2}V_{2-x}O_{11-x/2}$

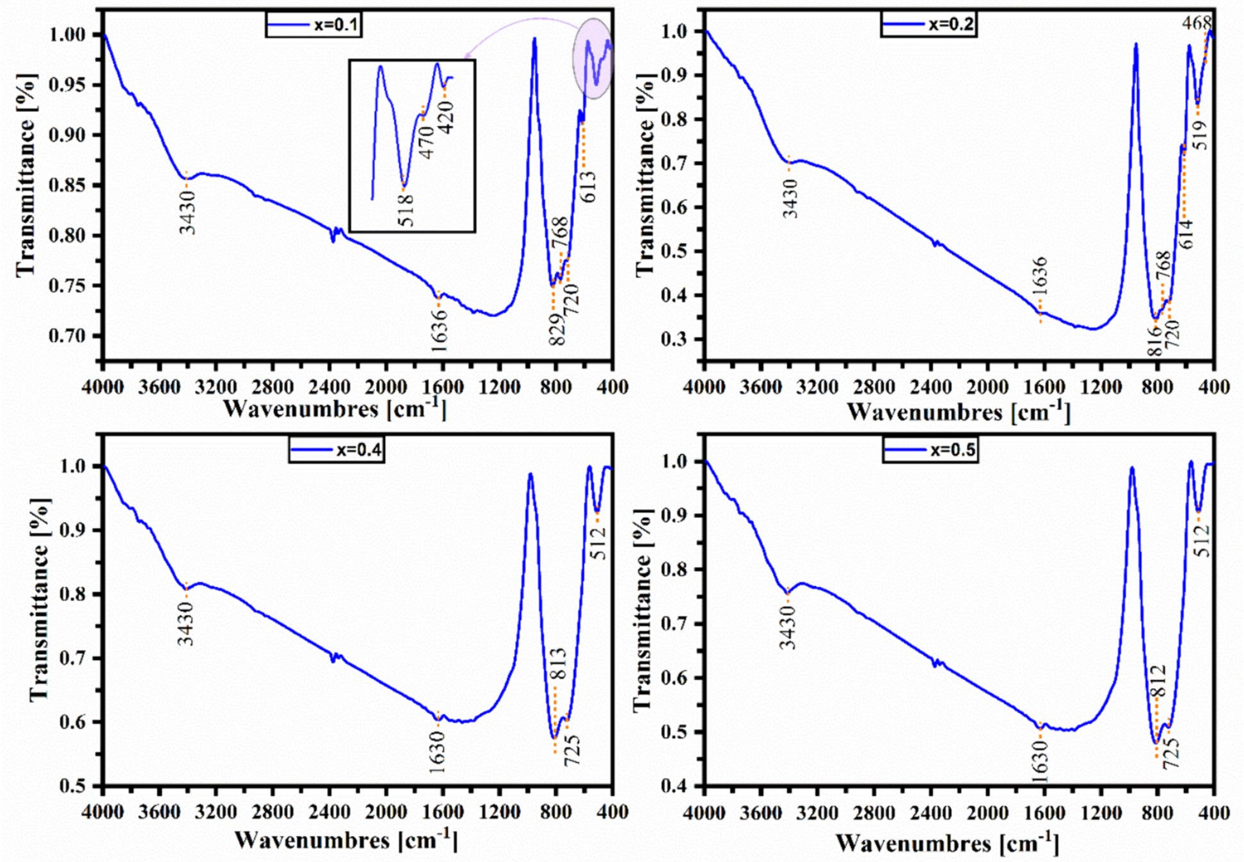

Fig. 7 Infrared spectra of $Bi_4Si_{x/2}Ge_{x/2}V_{2-x}O_{11-x/2}$ compounds

The Raman spectra of the α-monoclinic phase (samples with $x \le 0.3$) and the β-orthorhombic phase (samples with $x \ge 0.4$) exhibit similar spectral profiles in their respective compositional domains. The band observed at 156 cm^{-1} is attributed to the translational modes of the bismuth ions [3]. Within the spectral range of 200–580 cm^{-1}, the bands correspond to the bending modes of VO_6 octahedral coupled with bending vibrations of bismuth-oxygen polyhedral [17, 18, 34]. In the range of 600–870 cm^{-1}, the bands can be assigned to the symmetric and asymmetric stretching modes of the V–O bonds in tetrahedral VO_4 groups. The α-BiMeVOx phase of monoclinic type exhibits five bands at 640, 722, 776, 825, and 860 cm^{-1} [17, 18, 35], while the orthorhombic-type β-BiMeVOx phase displays three bands at 650, 738, and 838–845 cm^{-1}. The high wavenumber peak at 930 cm^{-1} is associated with the stretching vibrations in V–O-V chains [36]. As the content of silicon and germanium increases, the intensity of this peak decreases. In the case of the β-orthorhombic phase, the band at 930 cm^{-1} gradually shifts to lower frequencies (920 cm^{-1}) and merges with the main band as x increases. This phenomenon is attributed to the V–O stretching in a chain-like structure [17, 18], and the decrease in its intensity is due to the introduction of silicon and germanium into the network which dissociates the chains.

According to the relationship established by Hardcastle et al. [37] between Raman stretching frequencies (ν in cm^{-1}) and the length of the Vanadium–Oxygen bond, the V–O bond length was determined based on the strong band in the Raman spectrum. For the α-monoclinic phase ($x \le 0.3$), the Raman spectrum exhibits two distinct components at 860 cm^{-1} and 825 cm^{-1}, indicating the presence of two types of V–O bonds with significantly different lengths [ν_{as} (860 cm^{-1}); R = 1.6750 Å, ν_{as} (825 cm^{-1}); R = 1.6966 Å]. In contrast, a single broad component is observed in the spectrum of the β-orthorhombic phase. This contribution appears at 838 cm^{-1} for $x = 0.4$ and at 845 cm^{-1} for $x = 0.5$. The existence of a single band suggests the presence of a single type of V–O group [ν_{as} (838 cm^{-1}); R = 1.688 Å, [ν_{as} (845 cm^{-1}); R = 1.684 Å]. However, this group is likely to be located in a more disordered environment as suggested by the large bandwidth [16]. Notably, a greater increase in bond length is observed for the composition $x = 0.4$, which corresponds to the α → β phase transition. This observation aligns perfectly with the increase in lattice parameters observed when x transitions from 0.3 to 0.4, as revealed by the XRD results.

In order to study thermal behavior of the different phonon modes, temperature-dependent Raman spectra of compounds with $x = 0.1$ and $x = 0.4$ are presented in Figs. 9 and 10, respectively. For both compounds, one can observe that the Raman bands shift to lower frequencies and broaden when the temperature is increased, reflecting a standard thermal behavior of the phonons. For the compound with $x = 0.1$ (Fig. 9), the band at 930 cm^{-1} gradually shifts to 918 cm^{-1} at temperature 450 °C, signature of α to β phase transition, and merges with the band at 860 cm^{-1}, which is associated to the transition from β to γ phase. On the other hand, for the compound with $x = 0.4$ (Fig. 10), the band at 914 cm^{-1} is characteristic of the β phase. As the temperature is increased, this band gradually shifts to low frequency and merges with that located at 855 cm^{-1}, at temperature of 500 °C, indicating that the transition from β to γ phase occurs in the temperature range 450 °C—500 °C. These results are in good agreement with those of the temperature-dependent XRD and DTA studies.

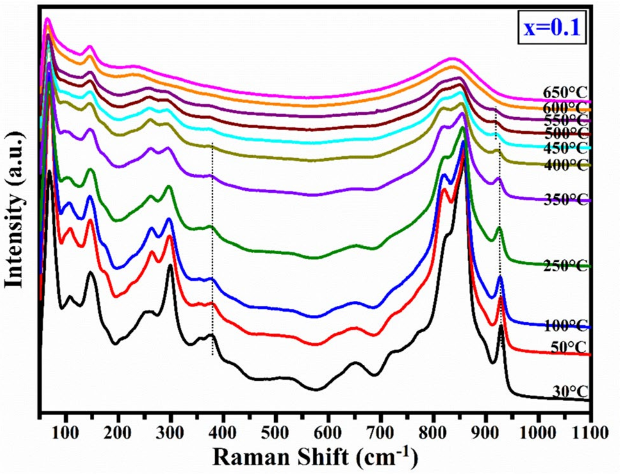

Fig. 9 Raman spectra of $Bi_4Si_{0.05}Ge_{0.05}V_{1.90}O_{10.95}$

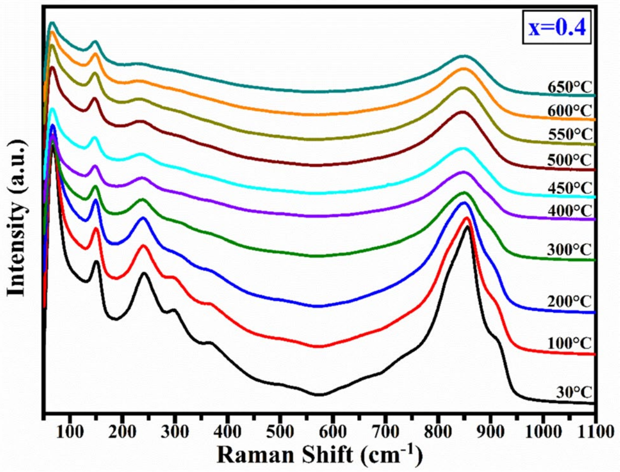

Fig. 10 Raman spectra of $Bi_4Si_{0.2}Ge_{0.2}V_{1.6}O_{10.8}$

The variation in the position of the V–O bonding band as a function of temperature, for $x = 0.1$ and 0.4, is shown in Fig. 11. The compound with $x = 0.1$, exhibits three linear regions attributed to the α → β and β → γ phase transitions around 450°C and 470°C, respectively. The compound with

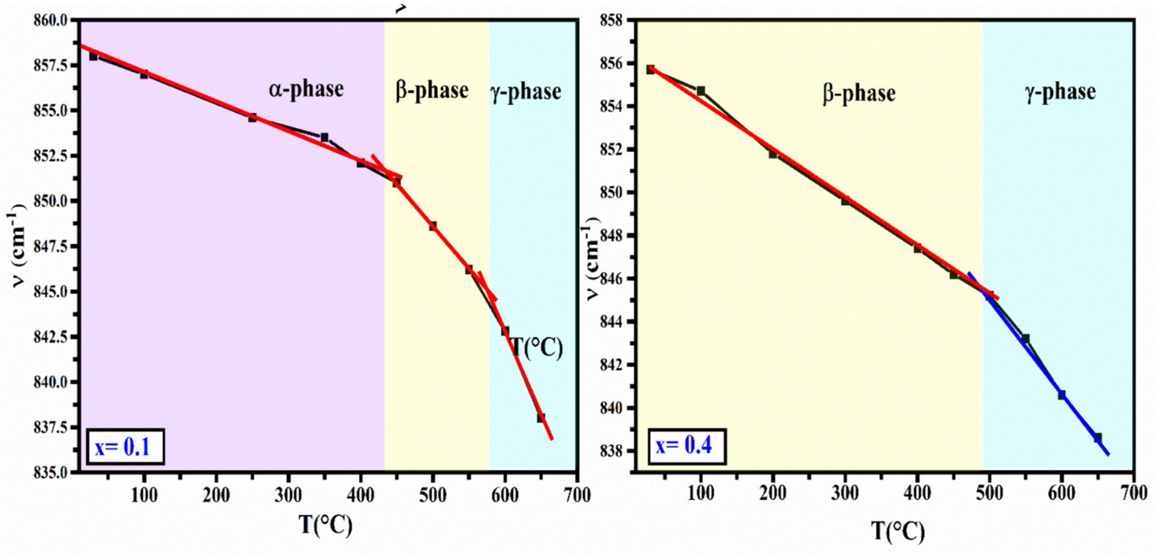

Fig. 11 The shift of the Raman ν_s(V–O) band as a function of temperature

x = 0.4, shows two linear regions related to the phase transition β → γ at about 500°C. These results allow us to determine a temperature-dependent equation such as:

$$\nu(T) = \nu_0 - kT$$

where ν_0 represents the frequency at 0°C and k is related to the degree of anharmonicity.

The values of ν_0 and k deduced from the linear fits are shown in Table 2. The frequency at 0°C is practically the same for both compounds. Furthermore, the coefficient value of the compound with x = 0.1 is slightly higher than that of the compound with x = 0.4, of the order of 0.224 and 0.195 cm^{-1}. °C^{-1}, respectively. It can be noted that the temperature coefficient varies only slightly despite the transition from a α-phase (x = 0.1) to a β-phase (x = 0.4).

3.3 SEM

Figure 12 displays SEM micrographs of $Bi_4Si_{x/2}Ge_{x/2}V_{2-x}O_{11-x/2}$ (0.1 ≤ x ≤ 0.5) pellets that were sintered at 840 °C for 5 h. The examined ceramics exhibit distinct and well-defined grains. Within the samples, residual porosity can be observed mainly between the grains. However, as the value of x increases, the ceramics exhibit a significantly lower degree of porosity and larger grain size with clearly visible grain boundaries. Notably, small-diameter pores are prominently present at the grain boundaries for samples with a doping level exceeding 15%, indicating that ceramics with higher doping level are more compact. Additionally, for x > 0.3, evidence of the beginning of fusion can be observed. Consequently, we infer that the melting temperature of the BiSiGeVOx solid solution decreases with increasing x. This peculiar microstructure phenomenon has also been reported in the BiMeVOx system [38, 39].

Table 3 presents the elemental analysis results obtained through Energy-Dispersive X-ray Spectroscopy (EDS). The analysis confirms the presence of Bi, V, Si, Ge, C, and O, which are uniformly distributed in the samples. The percentage of carbon atoms has been excluded from the table as it results from the sputtering process used during sample preparation for analysis. The atomic percentages of Si and Ge atoms show an increasing trend as the substitution rate (x) increases. In contrast, the percentage of V atoms decreases with increasing x. These findings indicate the successful substitution of vanadium by silicon and germanium in the solid solution.

Table 2 Raman frequency versus temperature for BiSiGeVOx

x = 0.1				
ν(T)	T ≤ 450 °C	450 °C < T ≤ 550 °C		T > 550 °C
	858.5—0.224 × T	**872.6- 0.048 × T**		**900.4—0.096 × T**
x = 0.4				
ν(T)	T ≤ 450 °C		T ≥ 500 °C	
	856.6—0.195 × T		**867.6—0.046 × T**	

Fig. 12 SEM micrographs of $Bi_4Si_{x/2}Ge_{x/2}V_{2-x}O_{11-x/2}$ ceramics: **a** x = 0.1, **b** x = 0.2, **c** x = 0.4 and **d**) x = 0.5

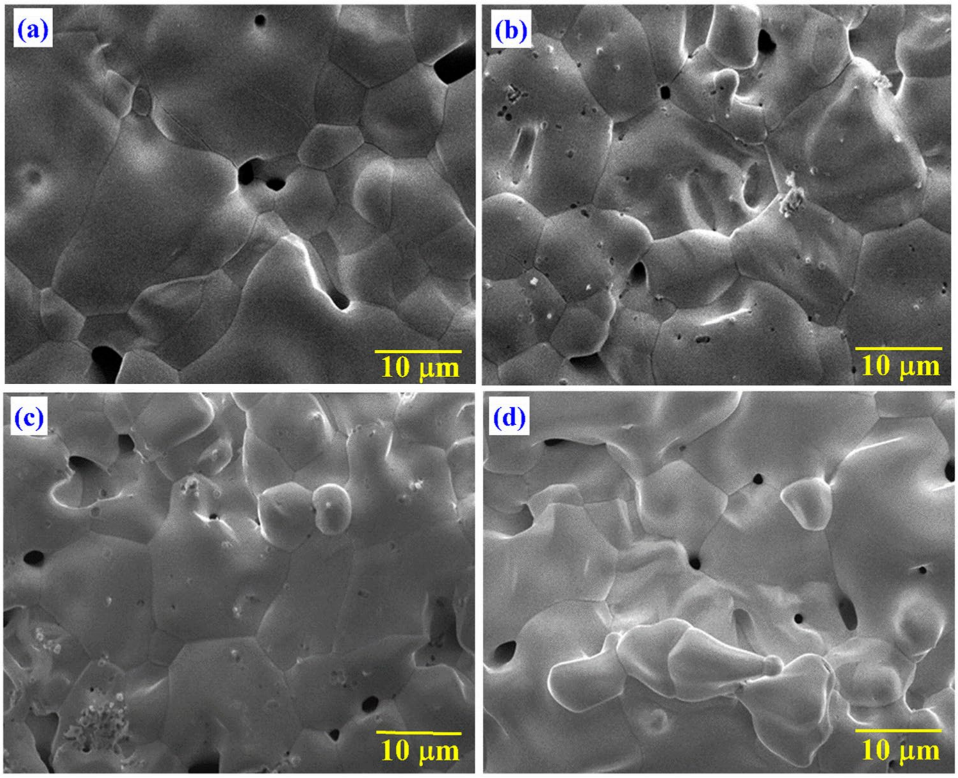

Table 3 Experimental percentages obtained by EDS (at %) analyses

Element	x = 0.1	x = 0.2	x = 0.3	x = 0.4	x = 0.5
O	56.18	55.89	58.61	63.43	66.69
Ge	0.25	0.52	0.90	1.28	2.63
Si	0.65	1.21	2.50	3.61	2.36
Bi	30.48	30.30	27.76	24.34	24.01
V	12.44	11.48	10.22	7.34	4.31

3.4 Optical Properties

Figure 13a, represented the diffuse reflectance spectra (DRS) of BiSiGeVOx in the 400–800 wavelength range. Direct band gaps (Eg) were determined by plotting $(F(R)\ h\nu)^2$ as a function of hν (1240/λ (nm)) and then extrapolating the linear segment of the graph to the x-axis, as shown in Fig. 13b. Absorption of visible light occurs at 596 nm, 587 nm and 574 nm for values of x = 0.1, 0.3 and 0.4, respectively. The absorption edge shifts to shorter wavelengths as the substitution rate increases. The bandgap energies Eg of x = 0.1, 0.3, and 0.4 have been estimated at 2.08, 2.11 eV, and 2.16 eV, respectively. These results allow us to conclude that both the

Fig. 13 UV–vis spectra of BiSiGeVOx: **a** Reflectance versus wavelength, and **b**) $(F(R)*h\nu)^2$ versus energy

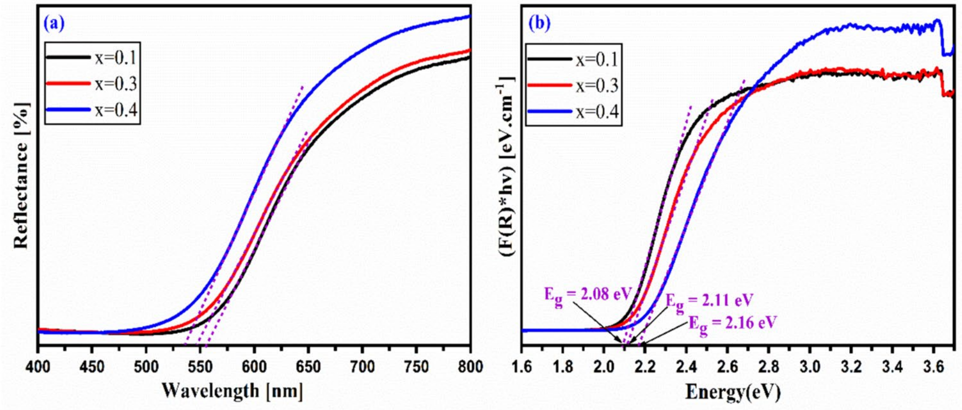

doping element and the stabilized phase have a very significant effect on the gap energy, as in the case of BiMeVOx solid solution [20, 21].

4 Conclusion

The synthesis of the Si-Ge co-doped solid solution $Bi_4Si_{x/2}Ge_{x/2}V_{2-x}O_{11-x/2}$ ($0.1 \leq x \leq 0.6$) is a key focus of this study. X-ray diffraction (XRD) analysis reveals the presence of two distinct phases in different composition ranges. The α phase, iso-structural of α-$Bi_4V_2O_{11}$, is observed for compositions ranging from 0.1 to 0.3, while the β phase, iso-structural of β-$Bi_4V_2O_{11}$, is present in the composition range of 0.4 to 0.5. Interestingly, the introduction of Si and Ge cations in this system does not contribute to the stabilization of the γ-tetragonal phase. DTA analysis showed two phase transitions α → β and β → γ for x = 0.1, a single transition β → γ for x = 0.4. To further investigate the phase transition, FTIR and Raman spectroscopy were performed at room temperature for various compositions. These vibrational studies provide additional evidence of the phase transition observed in the XRD analysis. Notably, the Raman spectra yielded V–O bond values for specific compositions. For example, at x = 0.3, the Raman spectrum exhibited a band at ν_{as} (860 cm^{-1}), corresponding to a V–O bond length of approximately 1.675 Å. Similarly, at x = 0.4, the Raman spectrum displayed a band at ν_{as} (838 cm^{-1}), corresponding to a V–O bond length of around 1.688 Å. This suggests that the β phase possesses relatively larger V–O bonds compared to the α phase. Overall, the synthesis and characterization results indicate the presence of distinct phases in the Si-Ge co-doped solid solution, with variations in the V–O bond lengths between the α and β phases. The diffuse reflectance spectroscopy spectra shows bandgap energy of 2.08–2.16 eV for the BiSiGeVOx solid solution, which shows that the double substitution of vanadium in $Bi_4V_2O_{11}$ leads to a narrower band gap for α- and β- substituted phases compared to that of the parent compound.

Acknowledgements The authors would like to express their gratitude to the Cadi Ayyad University Analysis and Characterization Center (CAC) for providing access to the materials characterization techniques used in this study.

Author Contributions A. AGNAOU: investigation, writing original draft, formal analysis; W. MHAIRA: helped the interpretation of results; R. ESSALIM: writing review and editing; M. ZAGHRIOUI: writing review and editing; T. CHARTIER: investigation; C. AUTRET: investigation; A. AMMAR: conceived the idea and supervision.

Funding None.

Data Availability No datasets were generated or analysed during the current study.

Declarations

Ethical Approval Not applicable.

Competing Interest The authors declare no competing interests.

References

1. Aurivillius B (1949) Mixed bismuth oxides with layer lattices. Arki Kemi 2
2. Kikuchi T, Watanabe A, Uchida K (1977) A family of mixed-layer type bismuth compounds. Mater Res Bull 12:299–304. https://doi.org/10.1016/0025-5408(77)90148-9
3. Ahsaine HA (2017) Etude de tungstate de bismuth (Bi, Lu)2WO6 : evolution des propriétés physicochimiques, luminescentes et photocatalytiques. Universite Ibn Zohr
4. Abraham F, Debreuille-Gresse MF, Mairesse G, Nowogrocki G (1988) Phase transitions and ionic conductivity in Bi4V2O11 an oxide with a layered structure. Solid State Ionics 28–30:529–532. https://doi.org/10.1016/S0167-2738(88)80096-1
5. Touboul M, Vachon C (1988) The Bi2O3-V2O5 system and crystal data about some bismuth vanadates. Thermochim Acta 133:61–66. https://doi.org/10.1016/0040-6031(88)87137-5
6. Mairesse G, Roussel P, Vannier RN et al (2003) Crystal structure determination of α-, β- and γ-Bi4V2O11 polymorphs. Part II: crystal structure of α-Bi4V2O11. Solid State Sci 5:861–869. https://doi.org/10.1016/S1293-2558(03)00016-5
7. Paydar MH, Hadian AM, Fafilek G (2001) Studies on preparation, characterisation and ion conductivity of TI-CU double substituted Bi4V2O11. J Eur Ceram Soc 21:1821–1824. https://doi.org/10.1016/S0955-2219(01)00123-6
8. Roy M, Sahu S, Barbar SK, Jangid S (2013) Synthesis, electrical and thermal properties of Bi4V2−xMexO11 (x = 0.0 and 0.02) ceramics. J Therm Anal Calorim 113:873–879. https://doi.org/10.1007/s10973-012-2833-1
9. Abrahams I (2003) A model for the mechanism of low temperature ionic conduction in divalent-substituted γ-BIMEVOXes. Solid State Ionics 157:139–145. https://doi.org/10.1016/S0167-2738(02)00201-1
10. Abrahams I, Bush AJ, Krok F et al (1998) Effects of preparation parameters on oxygen stoichiometry in Bi4V2O11−δ. J Mater Chem 8:1213–1217. https://doi.org/10.1039/a801614c
11. Boivin J (1998) Electrode-electrolyte BIMEVOX system for moderate temperature oxygen separation. Solid State Ionics 113–115:639–651. https://doi.org/10.1016/S0167-2738(98)00330-0
12. Löfberg A, Bodet H, Pirovano C et al (2006) Catalytic dense membranes of doped Bi4V2O11 (BIMEVOX) for selective partial oxidation: chemistry of defects versus catalysis. Top Catal 38:169–179. https://doi.org/10.1007/s11244-006-0082-x
13. Kant R, Singh K, Pandey O (2008) Synthesis and characterization of bismuth vanadate electrolyte material with aluminium doping for SOFC application. Int J Hydrogen Energy 33:455–462. https://doi.org/10.1016/j.ijhydene.2007.07.025
14. Karoum R, Pirovano C, Vannier RN et al (2009) Low temperature electrochemical catalysts using a BITAVOX electrolyte. Catal Today 146:359–366. https://doi.org/10.1016/j.cattod.2009.05.024
15. Chmielowiec J, Paściak G, BujŁo P (2009) BIMEVOX materials for application in SOFCS. Mater Sci Pol 27:1251–1256
16. Agnaou A, Mhaira W, Essalim R et al (2023) Correction: new silicon substituted BiMeVO x : synthesis and study of structural properties in relation to ionic conductivity. RSC Adv 13:8943–8943. https://doi.org/10.1039/D3RA90021E

17. Agnaou A, Mhaira W, Essalim R et al (2023) Structural study and ionic conductivity of Bi4V2−xSix/2Px/2O11−δ (0.0 ≤ x ≤ 0.5) compounds. J Solid State Chem 318:123730. https://doi.org/10.1016/j.jssc.2022.123730
18. Yue Y, Dzięgielewska A, Hull S et al (2022) Local structure in a tetravalent-substituent BIMEVOX system: BIGEVOX. J Mater Chem A 10:3793–3807. https://doi.org/10.1039/D1TA07547K
19. Anwar K, Naqvi FK, Beg S, Haneef S (2023) Photocatalytic degradation of MB dye and paracetamol drug, via hydrothermally synthesised praseodymium doped Bi4V2O11 nanoparticles. J Mol Struct 1272:134183. https://doi.org/10.1016/j.molstruc.2022.134183
20. Agnaou A, Mhaira W, Essalim R et al (2023) Effect of the doping element on the structure and UV–visible properties in the system Bi4V1.7(Si, Me)0.3O11-δ (Me = Si, P, Cu, and Co). Ionics (Kiel) 29:4923–4932. https://doi.org/10.1007/s11581-023-05185-7
21. Mhaira W, Agnaou A, Essalim R et al (2023) High-conducting Bi4V1.8Cu0.2-xSbxO10.7+3x/2 ceramics: structural, microstructural, electrical and optical properties. Ceram Int 49:39205–39213. https://doi.org/10.1016/j.ceramint.2023.09.264
22. Mhaira W, Agnaou A, Essalim R et al (2023) Structural, electrical, optical, and microstructural properties of Bi4V2-xCux/2Sbx/2O11−3x/4. J Solid State Electrochem 0–11. https://doi.org/10.1007/s10008-023-05768-4
23. Kharitonova EP, Voronkova VI (2007) Synthesis and electrical properties of Bi2V1−xGexO5+y solid solutions. Inorg Mater 43:55–59. https://doi.org/10.1134/S0020168507010128
24. Alga M, Ammar A, Essalim R et al (2005) Synthesis, sintering and electrical properties of P-doped Bi4V2O11 ceramics. Solid State Sci 7:1173–1179. https://doi.org/10.1016/j.solidstatesciences.2005.06.011
25. Shannon RD (1976) Revised effective ionic radii and systematic studies of interatomic distances in halides and chalcogenides. Acta Crystallogr Sect A 32:751–767. https://doi.org/10.1107/S0567739476001551
26. Agnaou A, Mhaira W, Essalim R et al (2023) Influence of Si4+ and Ga3+ doped in the BiSiGaVOx system on the structure and ionic conductivity. Silicon 1–8. https://doi.org/10.1007/s12633-023-02759-y
27. Ismunandar, Rusli R, Ramdan H (2011) Temperature dependent study of Bi2V1-xGaxO5.5 (x = 0.1 and 0.15) oxides. In: 2011 2nd International Conference on Instrumentation, Communications, Information Technology, and Biomedical Engineering. IEEE, pp 338–341
28. Rojas SS, De Souza JE, Andreeta MRB, Hernandes AC (2010) Influence of ceria addition on thermal properties and local structure of bismuth germanate glasses. J Non Cryst Solids 356:2942–2946. https://doi.org/10.1016/j.jnoncrysol.2010.05.101
29. Dimitrov V, Dimitriev Y, Montenero A (1994) IR spectra and structure of V2O5-GeO2-Bi2O3 glasses. J Non Cryst Solids 180:51–57. https://doi.org/10.1016/0022-3093(94)90396-4
30. Kumar B, Sharma R, Bhoi H et al (2023) Synthesis, structural, morphological and optical properties of environment friendly yellow inorganic pigment Bi4Zr3O12. Opt Mater (Amst) 142:114040. https://doi.org/10.1016/j.optmat.2023.114040
31. Essalim R, Ammar A, Zamama M, Mauvy F (2020) A study on structural properties, conductivity and FT-IR spectroscopy of Cu–Al doubly substituted Bi4V2O11. J Solid State Chem 288:121405. https://doi.org/10.1016/j.jssc.2020.121405
32. ElBatal FH, Marzouk MA, Abdelghany AM (2011) UV–visible and infrared absorption spectra of gamma irradiated V2O5-doped in sodium phosphate, lead phosphate, zinc phosphate glasses: a comparative study. J Non Cryst Solids 357:1027–1036. https://doi.org/10.1016/j.jnoncrysol.2010.11.040
33. Mhaira W, Agnaou A, Essalim R et al (2023) Effect of simultaneous Cu and Nb doping Bi4V2O11 on structural and electrical properties of Bi4V2−xCux/2Nbx/2O11−3x/4. J Solid State Chem 320:123878. https://doi.org/10.1016/j.jssc.2023.123878
34. Russu S (2008) High-throughput synthesis and characterization of vanadium mixed metal oxide pigments using synchroton radiation
35. Trzciński K, Borowska-Centkowska A, Sawczak M, Lisowska-Oleksiak A (2015) Photoelectrochemical properties of BIMEVOX (ME=Cu, Zn, Mn) electrodes in contact with aqueous electrolyte. Solid State Ionics 271:63–68. https://doi.org/10.1016/j.ssi.2014.10.008
36. Hardcastle FD, Wachs IE, Eckert H, Jefferson DA (1991) Vanadium(V) environments in bismuth vanadates: a structural investigation using Raman spectroscopy and solid state 51V NMR. J Solid State Chem 90:194–210. https://doi.org/10.1016/0022-4596(91)90135-5
37. Hardcastle F, Wachs I (1991) Determination of niobium-oxygen bond distances and bond orders by Raman spectroscopy. Solid State Ionics 45:201–213. https://doi.org/10.1016/0167-2738(91)90153-3
38. Wójcik NA, Polcyn K, Karczewski J et al (2022) High-conducting Bi4V2−xFexO11-δ ceramics containing Fe2O3 nanocrystals: structure and properties. J Eur Ceram Soc 42:5015–5022. https://doi.org/10.1016/j.jeurceramsoc.2022.05.012
39. Tripathy D, Saikia A, Tado GT, Pandey A (2019) Role of Al and Ti doping in modulating electrical properties of BIVOX system. J Adv Ceram 8:489–499. https://doi.org/10.1007/s40145-019-0329-1